

Revaluating ocean warming impacts on global phytoplankton

Michael J. Behrenfeld^{1*}, Robert T. O'Malley¹, Emmanuel S. Boss², Toby K. Westberry¹, Jason R. Graff¹, Kimberly H. Halsey³, Allen J. Milligan¹, David A. Siegel⁴ and Matthew B. Brown¹

Global satellite observations document expansions of the low-chlorophyll central ocean gyres and an overall inverse relationship between anomalies in sea surface temperature and phytoplankton chlorophyll concentrations. These findings can provide an invaluable glimpse into potential future ocean changes, but only if the story they tell is accurately interpreted. Chlorophyll is not simply a measure of phytoplankton biomass, but also registers changes in intracellular pigmentation arising from light-driven (photoacclimation) and nutrient-driven physiological responses. Here, we show that the photoacclimation response is an important component of temporal chlorophyll variability across the global ocean. This attribution implies that contemporary relationships between chlorophyll changes and ocean warming are not indicative of proportional changes in productivity, as light-driven decreases in chlorophyll can be associated with constant or even increased photosynthesis. Extension of these results to future change, however, requires further evaluation of how the multifaceted stressors of a warmer, higher-CO₂ world will impact plankton communities.

Ocean warming has been implicated as causing an expansion of the low-chlorophyll, low-productivity central ocean gyres^{1–3}. Satellite observations have also shown that broad ocean regions exhibit an inverse relationship between interannual and interdecadal changes in sea surface temperature (SST) and surface phytoplankton chlorophyll concentrations^{4–7}. In other words, chlorophyll tends to decrease when temperatures increase, or increase when temperatures decrease. If chlorophyll concentration is simplistically taken as a measure of phytoplankton biomass, then these findings imply a warmer future ocean may be accompanied by decreased phytoplankton stocks and productivity^{2,4,8–10}. However, the chlorophyll signal is not so easy to interpret. Chlorophyll concentrations also register physiological adjustments in cellular pigmentation arising from changes in upper ocean light and nutrient conditions^{11–14}. These physiological responses can potentially undermine earlier interpretations of the SST–chlorophyll relationship, and thus its extension to future ocean warming impacts^{5,7}.

Here, we show that physiological changes in cellular pigmentation are often the dominant cause of satellite-observed interannual variations in chlorophyll. This physiological signal includes a clear signature of phytoplankton responses to changing mixed-layer light conditions (that is, 'photoacclimation'). Our findings imply that temperature-correlated decreases in chlorophyll over large ocean areas are often not synonymous with equivalent decreased productivity. To arrive at this conclusion, it was necessary to first revisit mechanisms of light-regulated chlorophyll synthesis to construct a photoacclimation model applicable to the dynamic light environment of the upper ocean. The model was then evaluated against global phytoplankton carbon-to-chlorophyll ratio data (θ , a standard metric of cellular pigmentation), before assessing the contribution of photoacclimation to the satellite chlorophyll record. Our results yield a less dire interpretation of

contemporary ocean phytoplankton changes, provide new insight into chlorophyll synthesis regulation, and offer a revised description of photoacclimation that can benefit ocean ecosystem modelling, global productivity estimates, and evaluations of photoprotection in the light-saturated upper ocean.

Mechanisms of photoacclimation

Oxygenic photosynthesis involves coupled electron transport between two pigmented light-harvesting photosystems, termed PSII and PSI (Fig. 1a). An inner-membrane pool of plastoquinone (PQ) molecules functions as the electron shuttle between these photosystems, while simultaneously transporting protons across the photosynthetic membrane (which drives ATP synthesis). When phytoplankton are exposed to a range of increasing light intensities, their photosynthetic rate initially increases with light, but then saturates because ATP and reductant (NADPH) turnover become rate limiting (Fig. 1b). Consequently, electron transport between PSII and PSI progressively 'backs-up' as light increases, causing the PQ pool to become increasingly reduced (that is, in the form of plastoquinole, PQH₂ (Fig. 1b)). The ratio of these oxidized to reduced molecules (that is, the PQ pool 'redox state') thus provides a sensitive measure of the balance between the cell's light-harvesting 'machinery' and its capacity to utilize its photosynthetically generated ATP and NADPH. Phytoplankton use this signal (along with other correlated signals) to regulate chlorophyll synthesis^{15–18} (Supplementary Discussion). A predominantly oxidized PQ pool indicates that light harvesting is insufficient, so chlorophyll synthesis is upregulated. Conversely, a pool that is predominantly reduced indicates that chlorophyll concentration is too high, so synthesis is downregulated. This relationship between PQ redox state and chlorophyll synthesis is fundamental to photoacclimation models applied to satellite observations of surface ocean mixed-layer phytoplankton.

¹Department of Botany and Plant Pathology, Cordley Hall 2082, Oregon State University, Corvallis, Oregon 97331-2902, USA. ²School of Marine Sciences, 5706 Aubert Hall, University of Maine, Orono, Maine 04469-5741, USA. ³Department of Microbiology, 220 Nash Hall, Oregon State University, Corvallis, Oregon 97330, USA. ⁴Earth Research Institute and Department of Geography, University of California, Santa Barbara, California 93106-3060, USA.

*e-mail: mjb@science.oregonstate.edu

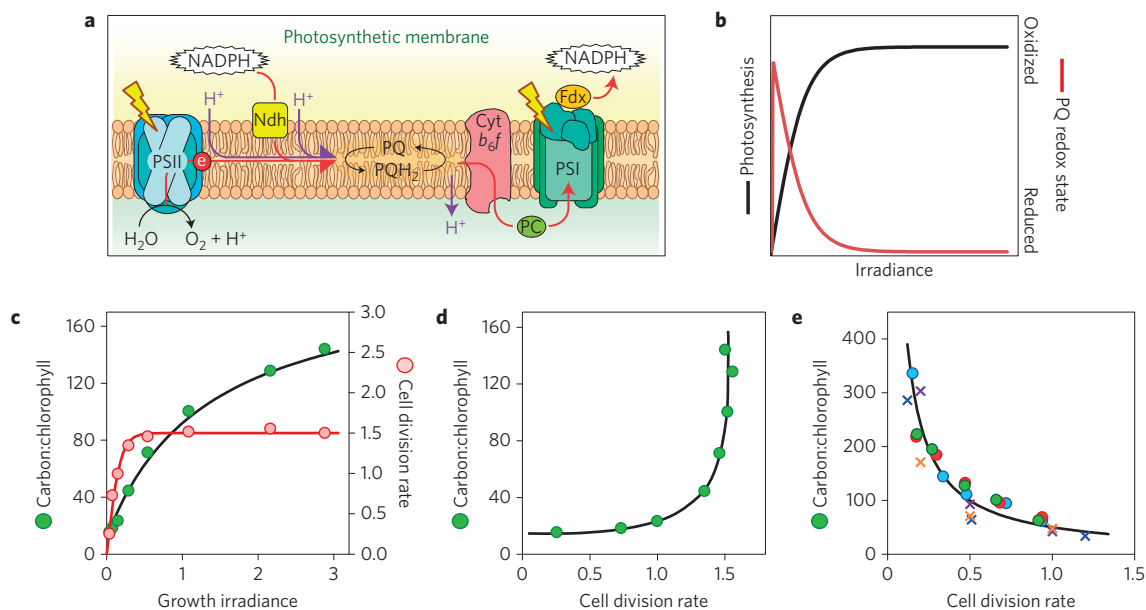


Figure 1 | Photophysiology of phytoplankton. **a**, Electron transport in photosynthetic membranes between water splitting at PSII and reductant (NADPH) formation after PSI. Also shown is electron transport in darkness from NADPH to the PQ pool through Ndh. PSII, photosystem II. PSI, photosystem I. Cyt b_{6f} , cytochrome b_{6f} complex. PQ, plastoquinone. PQH₂, plastoquinole. Fdx, ferredoxin. PC, plastocyanin. NADPH, nicotinamide adenine dinucleotide phosphate. NDH, NADPH dehydrogenase. Yellow 'lightning bolts' signify light absorption by PSII and PSI. **b**, Relationship between photosynthesis and incident irradiance (black line; relative). Photosynthesis initially increases in proportion to irradiance and then becomes light-saturated. The PQ pool is initially reduced in the dark, is oxidized on exposure to light, and then becomes progressively reduced with increasing light (red line; right axis). **c**, Changes in phytoplankton carbon-to-chlorophyll ratio (θ ; green symbols; left axis; g C (g Chl)⁻¹) and cell division rate (red symbols; right axis; d⁻¹) as a function of growth irradiance (mol photon m⁻² h⁻¹) as typically observed in nutrient-replete laboratory cultures. Data for *Dunaliella tertiolecta* from ref. 5. **d**, Relationship between θ and cell division rate for nutrient-replete phytoplankton based on data from **c**. **e**, Relationship between θ and cell division rate for steady-state nutrient-limited phytoplankton. Circles: *Thalassiosira weissflogii* under (blue) NO₃, (red) NH₄ and (green) PO₄ limitation. Crosses: NO₃-limited cultures of (blue) *Dunaliella tertiolecta*, (purple) *Thalassiosira weissflogii* and (orange) *Ostreococcus tauri*. Data from refs 11,47.

Whereas reduction of the PQ pool by bright light is widely recognized in photoacclimation models as a regulating factor for chlorophyll synthesis, far less attention has been given to PQ pool redox signalling under conditions of darkness. In the dark, NADPH is mobilized (through stored carbon catabolism) to reduce the PQ pool¹⁹ (Fig. 1a). This process has been documented over extensive open ocean regions through associated changes in phytoplankton fluorescence properties^{20–22}. In eukaryotic phytoplankton, this electron transport in the dark is referred to as 'chlororespiration'²³, whereas in prokaryotes it is simply referred to as 'cellular respiration'²⁴. A possible implication of this dark PQ redox change is that it may downregulate the chlorophyll synthesis signal. This effect has, to the best of our knowledge, never been considered in models of phytoplankton photoacclimation when deep mixing results in prolonged exposures to darkness.

Photoacclimation in laboratory cultures

Photoacclimation has been thoroughly examined in laboratory phytoplankton cultures^{11,12,14,25,26}, albeit under light conditions that rarely mimic natural deep-mixing layers. During these experiments, phytoplankton grown over a range of different light levels typically exhibit a strong decrease in θ with decreasing growth irradiance (that is, they become more pigmented; Fig. 1c, green symbols). This response, regulated by PQ redox sensing, is insufficient to prevent reductions in cell division rates at low light (Fig. 1c, red symbols). These parallel responses to changing growth irradiance can be summarized by replotting θ as a function of growth rate (Fig. 1d), thus illustrating how light-driven increases in division rate correspond to strong increases in θ . The opposite relationship is observed in laboratory studies of nutrient stress (Fig. 1e). Here, increases in division rate are associated with strong

decreases in θ because faster-growing cells need more chlorophyll (that is, lower θ) to meet demands for photosynthetic ATP and NADPH production.

The dependencies of θ on light and nutrient conditions are critical for understanding why satellites often observe chlorophyll to decrease with increasing temperature and stratification, and what these changes mean in terms of ocean production. More specifically, chlorophyll can decrease because of a decrease in biomass (lower productivity) or an increase in θ . If the change in θ is significant, it can result from an increase in nutrient stress (lower productivity; Fig. 1e) or an increase in growth irradiance (same or increased productivity; Fig. 1d). Interpreting the satellite chlorophyll record therefore requires separating the effects of biomass, nutrients and light, which in turn requires a robust description of photoacclimation for the surface ocean mixed-layer light environment.

Photoacclimation in the ocean's mixed layer

Over the photoperiod, incident sunlight in the mixed layer is attenuated (that is, decreases) exponentially with depth. During midday, photosynthesis near the surface is often light-saturated, meaning that the PQ pool is reduced and the signal for chlorophyll synthesis is 'off' (Fig. 2a). Supersaturating light levels within this 'high light zone' provide no additional redox information, but they do impact calculated values of the average light in the mixed layer. This discrepancy is one reason why average daily irradiance is not an appropriate descriptor of photoacclimation. Recognizing this limitation, an alternative approach has been to describe photoacclimation as a function of the median light level within a well-mixed surface layer (I_{ML} ; refs 7,13,27).

$$I_{ML} = \text{PAR} e^{-0.5K_d \text{MLD}} \quad (1)$$

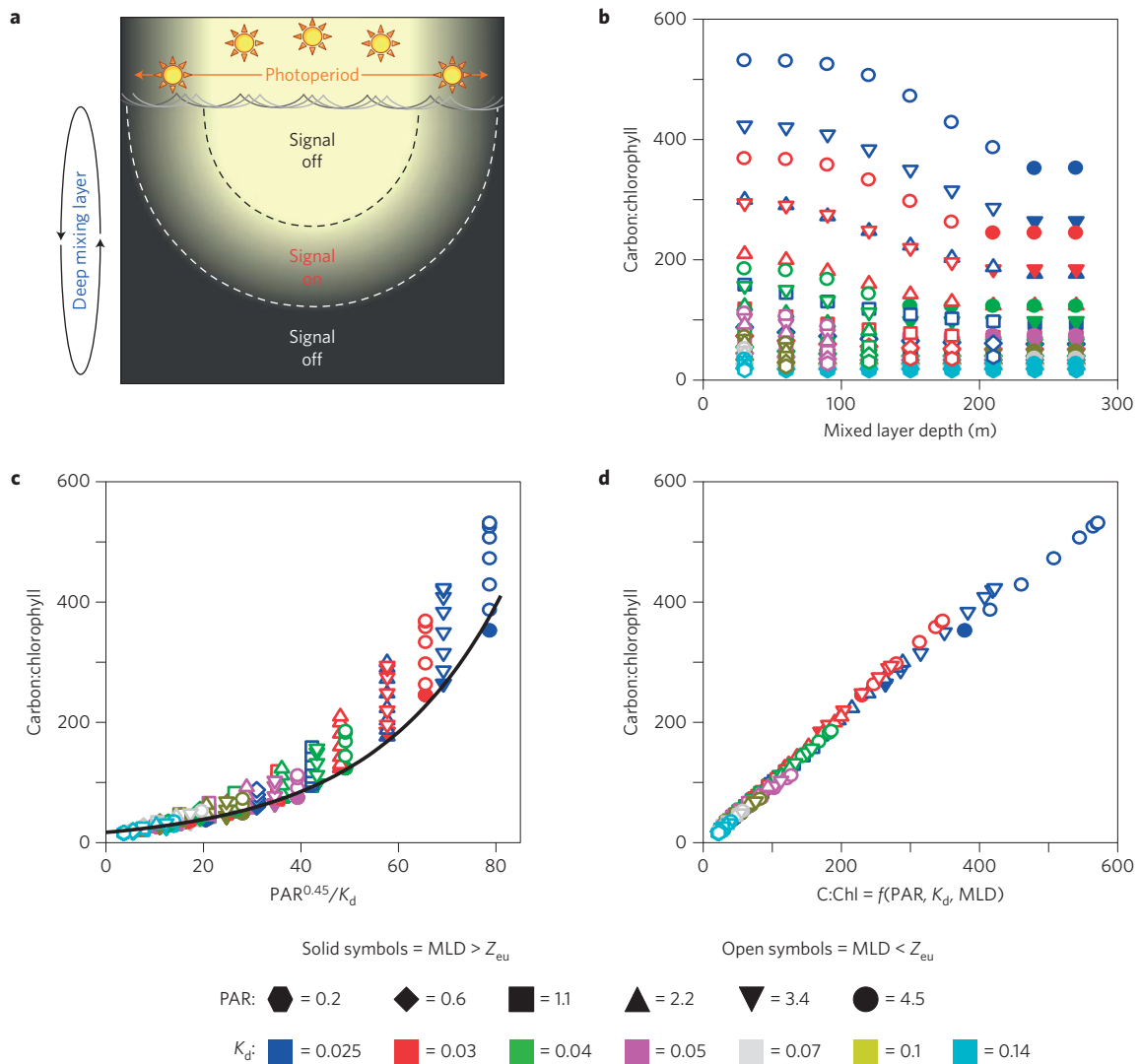


Figure 2 | Modelling photoacclimation in the surface ocean mixed layer. **a**, Schematic of the mixed-layer (indicated on left) light environment across the photoperiod (top). Redox state of the plastoquinone (PQ) pool is an important regulator of chlorophyll synthesis. Elevated incident sunlight during midday results in light-saturated photosynthesis in the upper photic layer, a reduced PQ pool (Fig. 1), and thus downregulation of chlorophyll synthesis (that is, ‘signal off’; area above black dashed line). Similarly, exposure to darkness below the photic depth (white dashed line) results in a biochemical reduction of the PQ pool (Fig. 1) and downregulation of chlorophyll synthesis. In between these two conditions, the PQ pool is oxidized and signals an upregulation of chlorophyll synthesis. Phytoplankton carbon-to-chlorophyll ratios (θ) reflect the balance between these ‘on’ and ‘off’ signals, which depends on mixed-layer depth (MLD; m), incident sunlight (PAR; mol of photons $m^{-2} h^{-1}$), and the attenuation coefficient for PAR (K_d ; m^{-1}). **b**, Steady-state values of θ ($g g^{-1}$) from the new photoacclimation model as a function of MLD (m). Solid symbols, deep-mixing scenarios where $MLD > Z_{eu}$; m. Open symbols, shallow-mixing scenarios where $MLD < Z_{eu}$. **c**, Relationship between model values of θ and $PAR^{0.45}/K_d$ (mol photon ($m h$) $^{-1}$). Black line, equation (2). **d**, Relationship between θ values for the full model (left axis) and from equations (2) and (3) (bottom axis). **b–d**, Symbol shapes and colours indicate model combinations of PAR and K_d , as defined in the key at the bottom of the figure.

where PAR is the photosynthetically active radiation (400–700 nm; mol photons $m^{-2} h^{-1}$), K_d is the attenuation coefficient (m^{-1}) for downwelling PAR, and MLD is the mixed-layer depth (m). This approach was intended to capture the midpoint light level where the signal for chlorophyll synthesis is ‘on’ for half of the mixing cycle and ‘off’ for the other half. However, neither the median nor the average mixed-layer light level account for the chlorophyll synthesis signal being ‘off’ in the dark (Fig. 2a). Consequently, these descriptors of photoacclimation can overestimate cellular chlorophyll levels when mixing depths exceed the photic zone depth (Z_{eu} ; the surface layer of the ocean supporting net photosynthesis).

Recognizing the complexity added by PQ redox signalling in the dark, we first revised the description of mixed-layer photoacclimation before evaluating its significance to global ocean

chlorophyll variability. To do this, we initially focused on conditions of deep mixing (that is, $MLD > Z_{eu}$) and then addressed the effects of mixed-layer shoaling within the photic zone (that is, $MLD < Z_{eu}$). For deep-mixing scenarios, time- and depth-resolved photosynthesis was calculated for a globally representative range in PAR (0.2–4.5 mol photons $m^{-2} h^{-1}$) and K_d (0.02–0.2 m^{-1}). We then determined the changes in the model photosynthesis–irradiance relationship necessary to yield a relationship between θ and net productivity consistent with laboratory findings (Fig. 1d). These deep-mixing solutions were then adjusted for shallow-mixing conditions ($MLD < Z_{eu}$) based on the relationship between θ and I_{ML} observed in open ocean regions where PAR and K_d are relatively constant (that is, where MLD changes are the primary driver of θ variability)^{13,27} (Supplementary Discussion).

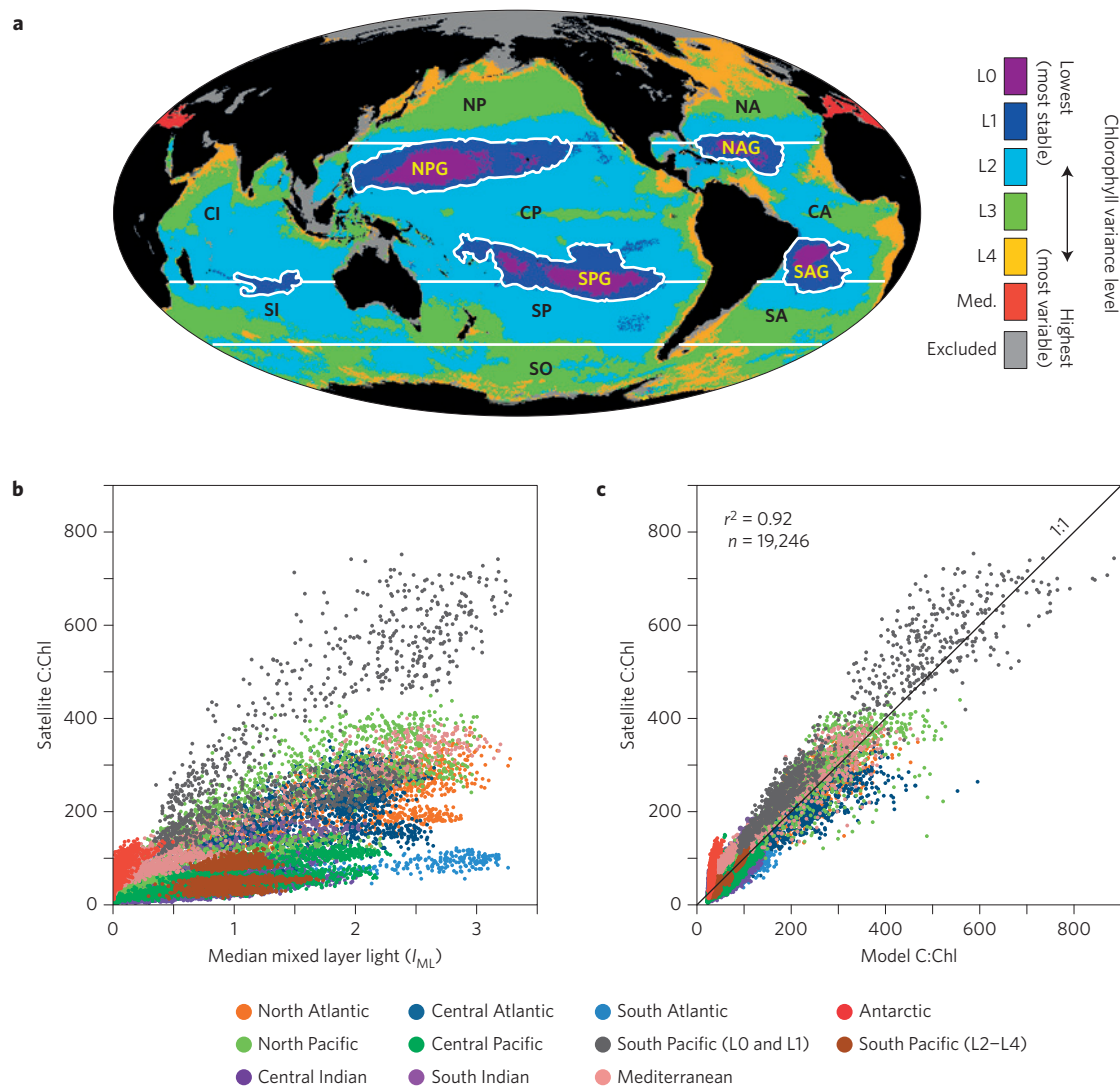


Figure 3 | Carbon-to-chlorophyll (θ) variability in the global ocean. **a, The 11-year record of MODIS Aqua 8-day resolution θ data were aggregated into 37 regional bins based on annual variability in chlorophyll, following ref. 13 (right-hand legend; L0, lowest variability (that is, most stable) waters; L4, highest variability waters). Basin designations are: NA, North Atlantic; CA, Central Atlantic; SA, South Atlantic; NP, North Pacific; CP, Central Pacific; SP, South Pacific; CI, Central Indian; SI, South Indian; SO, Southern Ocean; Med., Mediterranean; and Excluded, near-shore and polar waters excluded from the analyses. Central ocean gyres are indicated by the addition of 'G' to two-letter basin designation (for example, SPG, South Pacific Gyre). **b**, Relationship between satellite-observed values of θ (g C (g Chl) $^{-1}$) and median mixed-layer light levels (I_{ML} , mol photons $m^{-2} h^{-1}$). Colours, ocean basin as defined in the key at the bottom. South Pacific data for the low-variance L0 and L1 bins (black) are separated from higher-variance bins (brown) (see discussion in the main text). **c**, Relationship between satellite-observed θ and model values from equations (2) and (3).**

With this limited set of constraints, the model gives a wide range of steady-state solutions for θ (Fig. 2b), which we then analysed with respect to dependencies on PAR, K_d and MLD. For all deep-mixing conditions (solid symbols in Fig. 2c), model values for θ collapsed on a single relationship with $PAR^{0.45}/K_d$ (Fig. 2c, black line). The dependence here on $PAR^{0.45}$ results because daily-integrated water-column production initially increases linearly with PAR and then increases more slowly as a greater fraction of the photic zone becomes light-saturated over the photoperiod (that is, water-column productivity is a saturating function of incident PAR; refs 28,29). The dependence of θ on K_d in this relationship results because daily-integrated production for a given MLD and PAR varies inversely with the depth of the photic zone (in Fig. 2a, this region is the area above the dashed white line). The model then adjusts θ upwards from this $PAR^{0.45}/K_d$ solution when mixing is shallow, because less pigment is needed to sustain a given production rate (open symbols in Fig. 2c).

Results from our full model were used to define a simplified algorithm for application to satellite data. This photoacclimation algorithm is composed of a 'baseline' deep-mixing solution (θ_{DM} ; black line in Fig. 2c) and a shallow-mixing correction ($\Delta\theta_{SM}$). Thus, $\theta = \theta_{DM} \Delta\theta_{SM}$, where:

$$\theta_{DM} = c_1 e^{c_2 PAR^{0.45}/K_d} \quad (2)$$

with $c_1 = 19 \text{ g C (g Chl)}^{-1}$ and $c_2 = 0.038 \text{ m}^{-1}$. $\Delta\theta_{SM}$ has a value of 1 for $MLD \geq 6$ optical depths, whereas for shallower mixing it is calculated as:

$$\Delta\theta_{SM} = \frac{1 + e^{-0.15PAR}}{1 + e^{-3MLD}} \quad (3)$$

where the parameters in the exponents have units of $\text{m}^2 \text{ h (mol photon)}^{-1}$. The simplified algorithm (equations (2) and (3)) very effectively reproduces θ values from the full model for all

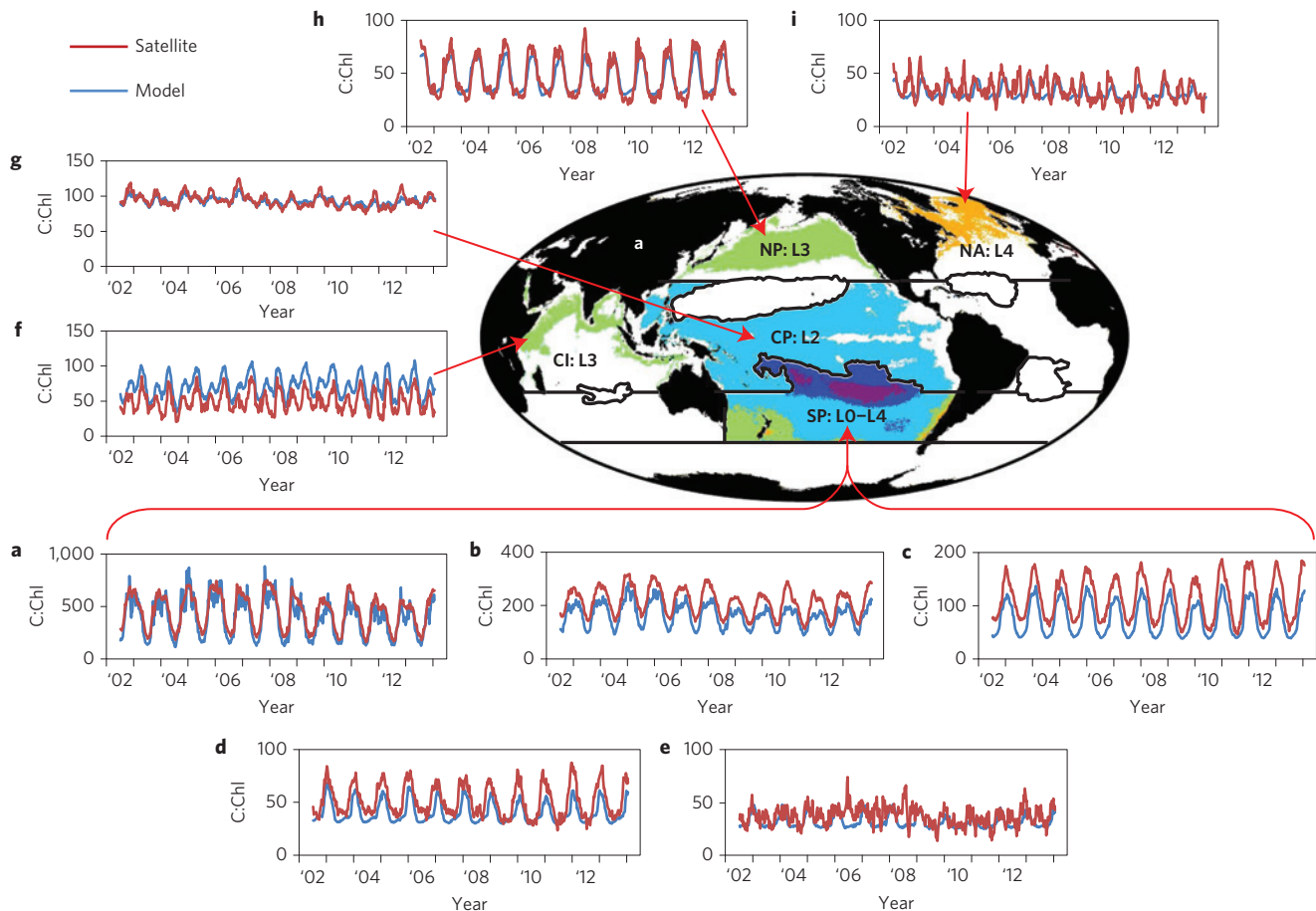


Figure 4 | Temporal patterns in satellite-observed carbon-to-chlorophyll (θ) and model-based variability attributable to photoacclimation.

a–e, Eleven-year records of θ (g C (g Chl)^{-1}) for the five South Pacific (SP) variance bins L0 (**a**), L1 (**b**), L2 (**c**), L3 (**d**) and L4 (**e**); note changing y-axis scales. **f**, L3 variance bin for the Central Indian (CI) region. **g**, L2 variance bin for the Central Pacific (CP) region. **h**, L3 variance bin for the North Pacific (NP) region. **i**, L4 variance bin for the North Atlantic (NA) region. Red lines, satellite θ record. Blue lines, model estimates (equations (2) and (3)) of θ variability due to photoacclimation.

combinations of PAR, K_d and MLD (Fig. 2d; $r^2 = 0.99$). The photoacclimation algorithm was then applied to an 11-year record of satellite ocean measurements from the MODerate resolution Imaging Spectroradiometer on Aqua (MODIS Aqua, July 2002 to January 2014) (Supplementary Discussion).

Global photoacclimation signature

Satellite measurements provide information on ocean ecosystem properties representative of the actively mixing surface layer, which can vary from tens to hundreds of metres. Retrieved chlorophyll concentrations reflect both phytoplankton abundance and cellular pigmentation (θ). An ability to partition chlorophyll into these two components has arisen from the development of spectral ocean colour inversion algorithms^{30–32} and subsequent assessments of phytoplankton carbon (C_{phyto}) from retrieved particulate backscattering coefficients (b_{bp} ; refs 13,27). Initially, C_{phyto} products were evaluated against indirect biomass proxies^{13,27,33,34}, but recent analytical field measurements of C_{phyto} (ref. 35) have now directly validated the satellite algorithm³⁶. Simultaneous retrieval of C_{phyto} and Chl allows global evaluations of phytoplankton θ variability.

MODIS Aqua 8-day resolution θ data were aggregated into 37 regional bins¹³ (Fig. 3a) and initially compared with median mixed-layer light values (I_{ML} ; Fig. 3b). The resultant relationship shows strong regional dependencies that illustrate how fundamental aspects of photoacclimation are insufficiently accounted for by I_{ML}

alone. In contrast, the photoacclimation model developed here (equations (2) and (3)) gives predicted values of θ that are far more consistent ($r^2 = 0.92$) with satellite observations for nearly all of the regional bins (Fig. 3c). High-latitude Southern Ocean data are clear outliers in this relationship (Fig. 3c; red symbols), probably reflecting biases in satellite ocean retrievals for this region that are well documented^{37,38}. The model also consistently underestimates observed θ values by $\sim 20\%$ for the lowest-variance regions of the South Pacific Gyre (SPG in Fig. 3a; black symbols in Fig. 3c), probably reflecting a particularly high Raman scattering contamination in b_{bp} retrievals for this region of the clearest natural waters on Earth³⁹.

The model-satellite data comparison shown in Fig. 3c indicates that, at the global scale, photoacclimation is a dominant factor driving θ variability of the mixed layer. The importance of this physiological response is also clear over the smaller dynamic range of θ variability within each regional bin. For example, the five South Pacific bins exhibit single-mode annual cycles in θ with peak values consistently occurring in summer, but with amplitudes that diminish from regions of low to high productivity (red lines in Fig. 4a–e, respectively; note, y-axis scale changes between panels). Both the timing and amplitude of these cycles are reliably reproduced by the photoacclimation model (4a–e, blue lines). In productive regions of the Central Indian Ocean, biannual monsoon seasons give rise to a multi-phase annual cycle in θ that contrasts with the South Pacific cycle but again has a strong

photoacclimation signature (Fig. 4f). A multi-phase annual cycle in θ is also observed over broad expanses of the temporally stable Central Pacific, but in this case the cycle has very low amplitude and is driven by Northern- and Southern-Hemisphere seasonal cycles in PAR and MLD encompassed by this expansive trans-equatorial bin (Fig. 4g). In the high-latitude North Pacific, θ exhibits a single-mode annual cycle (Fig. 4h), whereas at similar latitudes in the North Atlantic, θ values are comparatively low and have a less pronounced seasonal cycle reflecting offsetting responses to changing PAR, MLD and K_d (Fig. 4i). For all 37 regional bins, we find that photoacclimation is a primary contributor to observed temporal patterns in θ (Supplementary Fig. 8).

Photoacclimation in a changing climate

Satellite observations of global ocean phytoplankton began in 1978. From these initial measurements to the present, interannual trends in chlorophyll concentration have been observed that are related to climate forcings associated with basin-scale phenomena such as the El Niño–La Niña cycle, Pacific Decadal Oscillation, and Atlantic Meridional Oscillation^{4–6,40}. These interannual chlorophyll anomalies are small compared to the biomass-driven seasonal chlorophyll changes in bloom-forming ocean regions, for example, but they are particularly relevant to forecasts of future ocean warming impacts. In general, anomalies in chlorophyll and SST are inversely related, and this finding is often interpreted as implying that phytoplankton biomass and productivity decrease with ocean warming^{2,4,8–10}.

With an ability to separate chlorophyll changes into biomass and physiological components, it is now possible to evaluate the underlying drivers of interannual anomalies in chlorophyll. Although uncertainties remain in satellite chlorophyll and biomass estimates, what we find is that the interannual anomalies in chlorophyll for the MODIS record are predominantly (>55%) attributed to physiologically driven anomalies in θ , rather than changes in biomass, for over 75% of the global ocean area (Fig. 5a). For ~40% of the global area, changes in θ account for >85% of the chlorophyll anomalies (Fig. 5a). This strong contribution from physiological variability in θ encompasses a diversity of factors, including responses to mixed-layer light and nutrient conditions and shifts in phytoplankton community composition. However, the light-driven component of this variability can now be separated from other factors by applying our photoacclimation model. What we find is that the photoacclimation response accounts for between 10 and >80% of the observed global anomalies in θ for the MODIS record across 40% of the lower-latitude permanently stratified oceans and higher-latitude seasonal seas (Fig. 5b). What this means is that temporal anomalies in chlorophyll do not imply equivalent changes in mixed-layer production. This is because photoacclimation-driven changes in chlorophyll have the opposite relationship to production as nutrient-driven (or biomass-driven) changes in chlorophyll (Fig. 1d,e).

Outlook

Global satellite observations provide a remarkably powerful tool for understanding how ocean ecosystems function today and, ideally, for gaining insights on how these communities may change in the future. Our understanding of ocean ecology, however, inevitably changes (and will continue to change) as improvements are made in ocean colour analysis (for example, inversion algorithms) and descriptions of biological processes (for example, photoacclimation). Here, we have focused on the light-driven physiology of phytoplankton and how it impacts our interpretation of the satellite record. By advancing the description of photoacclimation, we have increased attribution of chlorophyll temporal anomalies to changes in mixed-layer light conditions, and consequently diminished attribution to other factors. Perhaps surprisingly, we find that biomass

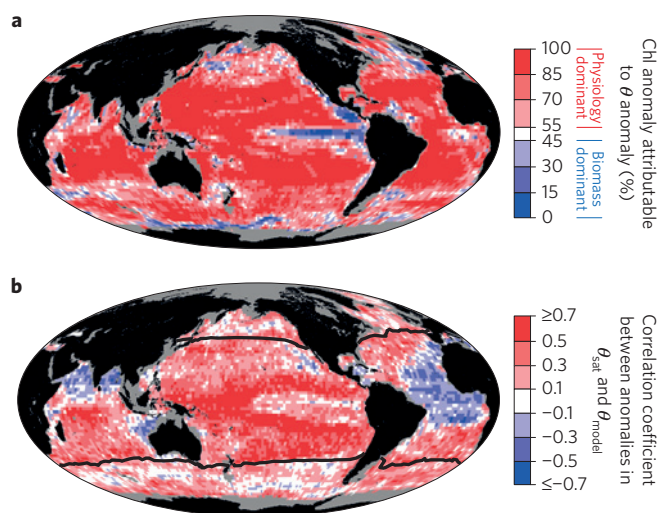


Figure 5 | Physiological contributions to global chlorophyll anomalies.

a, Percentage of observed chlorophyll anomalies (that is, difference between monthly values for a given year and the average monthly value for the 11-year MODIS Aqua record (July 2002–January 2014)) that is accounted for by observed monthly anomalies in θ . **b**, Linear, least-squares correlation coefficients (r) between observed anomalies in θ and model-predicted θ anomalies attributed to photoacclimation (r values of ≥ 0.3 have mean p -value significance levels of < 0.001). Black lines, annual mean SST of 15 °C, which approximately delineates the permanently stratified oceans from higher-latitude, seasonally deep-mixing regions¹³. Note that the large regions of negative correlations west of Africa and in the northern Indian Ocean (blue colours) correspond to regions with large atmospheric correction uncertainties for ocean retrievals.

changes dominate chlorophyll anomalies in only a few restricted regions (Fig. 5a), but this result is in part a consequence of the MODIS time frame. During the earlier Sea-viewing Wide Field-of-view Sensor (SeaWiFS) mission, a major El Niño–La Niña transition was recorded, during which event biomass changes were a primary driver of chlorophyll variability⁸.

Low-production central ocean gyres and high-latitude bloom-forming regions can have vastly different chlorophyll concentrations that reflect, to first order, differences in phytoplankton biomass driven by plankton predator–prey interactions⁴¹ and mixed-layer nutrient loading⁷. However, a central message from the present investigation is that physiological factors must always be considered when evaluating chlorophyll data, particularly in the interpretation of interannual chlorophyll anomalies. This conclusion raises the question, how are previously reported inverse relationships between chlorophyll and SST anomalies mechanistically linked to phytoplankton physiology? Part of the answer to this question is that SST changes are often linked to changes in surface-layer mixing. Changes in mixed-layer depth can alter the light level to which phytoplankton are photoacclimated and may or may not influence surface-layer nutrient concentrations⁴². Both of these mechanisms impact phytoplankton physiology, and thus θ . In the present study, we quantify the photoacclimation response but also show that other factors can dominate interannual anomalies in θ (Fig. 5b). A challenge for future studies is to disentangle the remaining unexplained θ variability into contributions from, for example, nutrient changes, physical advection⁴², community composition, and satellite retrieval errors. Such a partitioning will significantly refine our understanding of ocean ecosystem responses to contemporary climate variability.

Phytoplankton inhabiting the surface ocean mixed layer have evolved a diverse set of physiological tools to negotiate their highly

variable growth environment. Photoacclimation is an essential component of this plasticity, and the continued mechanistic refinement of its description is critical not only for the interpretation of global chlorophyll changes, but also assessments of ocean productivity²⁷, organic carbon export from the surface ocean to depth⁴³, and performance evaluations of modern coupled ocean ecosystem models⁴⁴. Accurate photoacclimation models are also requisite for quantifying phytoplankton photoprotection under supersaturating light (that is, nonphotochemical quenching), which is the dominant signal registered in satellite-retrieved chlorophyll fluorescence quantum yield data⁴⁵. Here, we call new attention to the potential importance of dark exposure periods during deep mixing on regulatory mechanisms of photoacclimation. Recognition of PQ pool redox changes in the dark was fundamental to the development of our revised photoacclimation model. It might be further suggested that regulation of photoacclimation is one role of chlororespiration in eukaryotes, the function of which has been debated²³.

By accounting for the photoacclimation response, we can conclude that temporal anomalies in surface chlorophyll over-represent associated changes in mixed-layer productivity for the MODIS record. However, caution is needed when extrapolating this conclusion to water-column-integrated production or the potential impacts of future ocean warming. With respect to the former, a shallowing of the mixed layer can drive an increase in surface-layer photosynthesis, but simultaneously causes a proportional expansion in the light-limited phytoplankton population below the mixed layer. These coincident effects have counteracting impacts on depth-integrated production. With respect to future warming, it is important to remember that the satellite record captures global phytoplankton responses only to present changes in the surface ocean environment, which are not fully reflective of the multifaceted changes anticipated with upcoming climate change. Understanding the integrated ramifications of these future changes will require a comprehensive and multi-stressor assessment of plankton ecosystem responses and feedbacks⁴⁶.

Received 10 June 2015; accepted 22 September 2015;
published online 26 October 2015

References

- Irwin, A. J. & Oliver, M. J. Are ocean deserts getting larger? *Geophys. Res. Lett.* **36**, L18609 (2009).
- McClain, C. R., Signorini, S. R. & Christian, J. R. Subtropical gyre variability observed by ocean-color satellites. *Deep-Sea Res. II* **51**, 281–301 (2004).
- Polovina, J. J., Howell, E. A. & Abecassis, M. Ocean's least productive waters are expanding. *Geophys. Res. Lett.* **35**, 3618 (2008).
- Behrenfeld, M. J. *et al.* Climate-driven trends in contemporary ocean productivity. *Nature* **444**, 752–755 (2006).
- Behrenfeld, M. J., Halsey, K. & Milligan, A. Evolved physiological responses of phytoplankton to their integrated growth environment. *Phil. Trans. R. Soc. B* **363**, 2687–2703 (2008).
- Martinez, E., Antoine, D., D'Ortenzio, F. & Gentili, B. Climate-driven basin-scale decadal oscillations of oceanic phytoplankton. *Science* **326**, 1253–1256 (2009).
- Siegel, D. A. *et al.* Regional to global assessments of phytoplankton dynamics from the SeaWiFS mission. *Remote Sens. Environ.* **135**, 77–91 (2013).
- Gregg, W. W., Casey, N. W. & McClain, C. R. Recent trends in global ocean chlorophyll. *Geophys. Res. Lett.* **32**, L03606 (2005).
- Kahru, M., Kudela, R., Manzano-Sarabia, M. & Mitchell, B. G. Trends in primary production in the California Current detected with satellite data. *J. Geophys. Res.* **114**, C02004, 10340 (2009).
- Boyce, D. G., Lewis, M. L. & Worm, B. Global phytoplankton decline over the past century. *Nature* **466**, 591–596 (2010).
- Laws, E. A. & Bannister, T. T. Nutrient- and light-limited growth of *Thalassiosira fluviatilis* in continuous culture, with implications for phytoplankton growth in the ocean. *Limnol. Oceanogr.* **25**, 457–473 (1980).
- Geider, R. J. Light and temperature dependence of the carbon to chlorophyll ratio in microalgae and cyanobacteria: Implications for physiology and growth of phytoplankton. *New Phytol.* **106**, 1–34 (1987).
- Behrenfeld, M. J., Boss, E., Siegel, D. A. & Shea, D. M. Carbon-based ocean productivity and phytoplankton physiology from space. *Glob. Biogeochem. Cycles* **19**, GB1006 (2005).
- Halsey, K. H. & Jones, B. M. Phytoplankton strategies for photosynthetic energy allocation. *Annu. Rev. Mar. Sci.* **7**, 265–297 (2015).
- Escoubas, J. *et al.* Light intensity regulation of cab gene transcription is signaled by the redox state of the plastoquinone pool. *Proc. Natl Acad. Sci. USA* **92**, 10237–10241 (1995).
- Durnford, D. G. & Falkowski, P. G. Chloroplast redox regulation of nuclear gene transcription during photoacclimation. *Photosynth. Res.* **53**, 229–241 (1997).
- Oelze, M., Kandlbinder, A. & Dietz, K. Redox regulation and overreduction control in the photosynthesizing cell: Complexity in redox networks. *Biochim. Biophys.* **1780**, 1261–1272 (2008).
- Pfannschmidt, T. & Yang, C. The hidden function of photosynthesis: A sensing system for environmental conditions that regulates plant acclimation responses. *Protoplasma* **249**, S125–S136 (2012).
- Cooley, J., Howitt, C. & Vermaas, W. Succinate: Quinol oxidoreductases in the cyanobacterium *Synechocystis* sp. strain PCC 6803: Presence and function in metabolism and electron transport. *J. Bacteriol.* **182**, 714–722 (2000).
- Behrenfeld, M. J. *et al.* Controls on tropical Pacific Ocean productivity revealed through nutrient stress diagnostics. *Nature* **442**, 1025–1028 (2006).
- Behrenfeld, M. J. & Milligan, A. J. Photophysiological expressions of iron stress in phytoplankton. *Annu. Rev. Mar. Sci.* **5**, 217–246 (2013).
- Fujiki, T., Hosaka, T., Kimoto, H., Ishimaru, T. & Saino, T. *In situ* observations of phytoplankton productivity by an underwater profiling buoy system: Use of fast repetition rate fluorometry. *Mar. Ecol. Prog. Ser.* **353**, 81–88 (2008).
- Peltier, G. & Cournac, L. Chlororespiration. *Ann. Rev. Plant Biol.* **53**, 523–550 (2002).
- Vermaas, W. F. J. *Encyclopedia of Life Sciences* (John Wiley, 2001).
- Behrenfeld, M. J., Marañón, E., Siegel, D. A. & Hooker, S. B. A photoacclimation and nutrient based model of light-saturated photosynthesis for quantifying oceanic primary production. *Mar. Ecol. Prog. Ser.* **228**, 103–117 (2002).
- MacIntyre, H. L., Kana, T. M., Anning, T. & Geider, R. J. Photoacclimation of photosynthesis irradiance response curves and photosynthetic pigments in microalgae and cyanobacteria. *J. Phycol.* **38**, 17–38 (2002).
- Westberry, T. K., Behrenfeld, M. J., Siegel, D. A. & Boss, E. Carbon-based primary productivity modeling with vertically resolved photoacclimation. *Glob. Biogeochem. Cycles* **22**, GB2024 (2008).
- Platt, T. & Sathyendranath, S. Estimators of primary production for interpretation of remotely sensed data on ocean color. *J. Geophys. Res.* **98**, 14561–14567 (1993).
- Behrenfeld, M. J. & Falkowski, P. G. A consumer's guide to phytoplankton primary productivity models. *Limnol. Oceanogr.* **42**, 1479–1491 (1997).
- Roesler, C. S. & Perry, M. J. *In situ* phytoplankton absorption, fluorescence emission, and particulate backscattering spectra determined from reflectance. *J. Geophys. Res.* **100**, 13279–13294 (1995).
- Maritorena, S., Siegel, D. A. & Peterson, A. R. Optimization of a semianalytical ocean color model for global-scale applications. *Appl. Opt.* **41**, 2705–2714 (2002).
- Lee, Z. P., Carder, K. L. & Arnone, R. A. Deriving inherent optical properties from water color: A multi-band quasi-analytical algorithm for optically deep waters. *Appl. Opt.* **41**, 5755–5772 (2002).
- Huot, Y., Morel, A., Twardowski, M. S., Stramski, D. & Reynolds, R. A. Particle optical backscattering along a chlorophyll gradient in the upper layer of the eastern South Pacific Ocean. *Biogeosciences* **5**, 495–507 (2008).
- Martinez-Vicente, V., Dall'olmo, G., Tarran, G., Boss, E. & Sathyendranath, S. Optical backscattering is correlated with phytoplankton carbon across the Atlantic Ocean. *Geophys. Res. Lett.* **40**, 1154–1158 (2013).
- Graff, J. R., Milligan, A. J. & Behrenfeld, M. J. The measurement of phytoplankton biomass using flow-cytometric sorting and elemental analysis of carbon. *Limnol. Oceanogr. Method* **10**, 910–920 (2012).
- Graff, J. R. *et al.* Analytical phytoplankton carbon measurements spanning diverse ecosystems. *Deep-Sea Res. I* **102**, 16–25 (2015).
- Mitchell, B. G. & Kahru, M. Bio-optical algorithms for ADEOS-2 GLI. *J. Remote Sens. Soc. Jpn* **29**, 80–85 (2009).
- Gregg, W. W. & Casey, N. W. Global and regional evaluation of the SeaWiFS chlorophyll data set. *Remote Sens. Environ.* **93**, 463–479 (2004).
- Westberry, T. K., Boss, E. & Lee, Z. The influence of Raman scattering on ocean color inversion models. *Appl. Opt.* **52**, 5552–5561 (2013).
- Henson, S. A. *et al.* Detection of anthropogenic climate change in satellite records of ocean chlorophyll and productivity. *Biogeosciences* **7**, 621–640 (2010).
- Behrenfeld, M. J. Climate-mediated dance of the plankton. *Nature Clim. Change* **4**, 880–887 (2014).

42. Lozier, M. S., Dave, A. C., Palter, J. B., Gerber, L. M. & Barber, R. T. On the relationship between stratification and primary productivity in the North Atlantic. *Geophys. Res. Lett.* **38**, L18609 (2011).
43. Siegel, D. A. *et al.* Global assessment of ocean carbon export using food-web models and satellite observations. *Glob. Biogeochem. Cycles* **28**, 181–196 (2014).
44. Doney, S. C. *et al.* Skill metrics for confronting global upper ocean ecosystem-biogeochemistry models against field and remote sensing data. *J. Mar. Syst.* **76**, 95–112 (2009).
45. Behrenfeld, M. J. *et al.* Satellite-detected fluorescence reveals global physiology of ocean phytoplankton. *Biogeosciences* **6**, 779–794 (2009).
46. Boyd, P. W., Lennartz, S. T., Glover, D. M. & Doney, S. C. Biological ramifications of climate-change-mediated oceanic multi-stressors. *Nature Clim. Change* **5**, 71–79 (2015).
47. Halsey, K. H., Milligan, A. J. & Behrenfeld, M. J. Contrasting strategies of photosynthetic energy utilization drive lifestyle strategies in ecologically important picoeukaryotes. *Metabolites* **4**, 260–280 (2014).

Acknowledgements

This work was supported by the National Aeronautics and Space Administration's Ocean Biology and Biogeochemistry Program.

Author contributions

M.J.B. designed the study; M.J.B., R.T.O'M. and E.S.B. conducted satellite data analyses and photoacclimation model development; M.J.B. and R.T.O'M. prepared display items; M.J.B. wrote the manuscript with contributions from all authors.

Additional information

Supplementary information is available in the [online version of the paper](#). Reprints and permissions information is available online at www.nature.com/reprints. Correspondence and requests for materials should be addressed to M.J.B.

Competing financial interests

The authors declare no competing financial interests.